Propagation Constant Determination in Microwave Fixture De-embedding Procedure

JYOTI P. MONDAL, MEMBER, IEEE, AND TZU-HUNG CHEN, MEMBER, IEEE

Abstract—**An improper choice of dimensions for the standards used in the microwave de-embedding procedure will cause errors in the determination of the propagation constant. This leads to unrealistic values for the attenuation constant, which in turn causes errors in the de-embedded results. Proper selection of dimensions is made to minimize such errors. Physically realistic values are obtained with this selection.**

I. Introduction

IN RECENT YEARS, a number of ways have been reported in the literature to de-embed the S parameters of an embedded device from the microwave test fixture. The well-known delay line techniques [1]–[3] have been successfully applied to remove most of the fixture-related uncertainties during measurement. There have been attempts to characterize the fixture through modeling [4], [5] and apply the model for device de-embedding. In-fixture [6], [7] calibration techniques are also used to improve the accuracy of the measurement. A number of techniques [8] have been discussed for measuring the S parameters of a fixtured device using the HP8510 network analyzer.

The present article is similar in basic philosophy to that of TSD; we have used one in-fixture standard for either of the two ports and selected the dimensions of the standard through lines in a way that will minimize the measurement errors and yield realistic values for the propagation constant. Throughout the analysis it is assumed that a TEM mode is propagating in the frequency range of interest.

II. Analysis

The three standards which will be measured are shown in Fig. 1. It has been already pointed out [3] that any discontinuity effects due to a different characteristic impedance of the standards (other than the system reference impedance, usually 50 Ω) are absorbed by the end launchers. It is also easy to show that the transitional discontinuities, between the launcher pins and the microstrip line in our case, also get absorbed in the end launchers. The combined effect of the above two discontinuities is to modify the de-embedded S parameters of the end launchers. Since, as we will find afterwards, the ultimate de-embedded result of the device S parameters depends on the difference in length of the various standards, we can safely take the physical lengths of the standards for calculating the electrical lengths of the lines (if we choose the line lengths sufficiently long so that the transitional discontinuities do not overlap). The ultimate effectiveness of such a deembedding procedure very much depends on the accuracy with which the transitional discontinuities are reproduced. As we will find with the reported results, the procedure works quite well even with the assumed constraints that the discontinuities are the same from one carrier to the other. One way to minimize such uncertainties, due to junction capacitance and inductance between launcher pin and the microstrip line, is to choose the microstrip line width very close to the diameter of the pin, and any change in the impedance of the line due to change in width is simply absorbed as a transformer in the S parameters of the launchers. With reference to Fig. 1, the propagation constant of the through lines can be shown to be

$$\gamma = \frac{\ln\left(\dfrac{A \pm \sqrt{A^2-4}}{2}\right)}{(l_1 - l_2)} \tag{1}$$

where

$A = (T11M1 \cdot T22M2 + T11M2 \cdot T22M1) - (T21M1 \cdot T12M2 + T12M1 \cdot T21M2)$,

$\gamma = \alpha + j\beta = \alpha + j\dfrac{2\pi}{\lambda_{\text{eff}}}$,

λ_{eff} effective wavelength in the medium,

$l_1 - l_2$ difference in through line lengths.

Manuscript received May 11, 1987; revised August 31, 1987. This work was supported in part by the GE Independent Research and Development Fund.

J. P. Mondal is with the Electronics Laboratory, General Electric Company, Electronics Park, Syracuse, NY 13221.

T.-H. Chen was with the Electronics Laboratory, General Electric Company, Syracuse, NY. He is now with the Microwave Semiconductor Corporation, Somerset, NJ 08873.

IEEE Log Number 8719434.

The measured scattering chain parameters are

$$T11M1 = \frac{S11M1 \cdot S22M1 - (S12M1)^2}{S12M1}$$

$$T21M1 = -\frac{S22M1}{S12M1}$$

$$T12M1 = \frac{S11M1}{S12M1}$$

$$T22M1 = 1/(S12M1)$$

$$T11M2 = -\frac{S11M2 \cdot S22M2 - (S12M2)^2}{S12M2}$$

$$T21M2 = -\frac{S22M2}{S12M2}$$

$$T12M2 = \frac{S11M2}{S12M2}$$

$$T22M2 = 1/(S12M2).$$

Equation (1) is equivalent to (18) in [1]. The arguments of "ln" in (1) are reciprocal to each other. If $l_1 > l_2$, the correct solution has the positive sign, and the range of validity of this solution is given by

$$0 < \arg(A) < \frac{\pi}{2} \qquad \left(\text{or, } -\frac{\pi}{2} < \arg(A) < 0 \text{ for } l_1 < l_2\right). \tag{2}$$

The inequality (2) ensures a unique solution to expression (1). In terms of standard dimensions, (2) translates into $|l_1 - l_2| < \lambda_{\text{eff}}/4$, for α small (Appendix I). For

$$\frac{\lambda e}{4} < (l_1 - l_2) < \frac{\lambda e}{2}$$

the proper choice in (1) is the negative sign and

$$\frac{\pi}{2} < \arg(A) < \pi. \tag{3}$$

The expressions for the de-embedded device S parameters can be derived from the cascaded scattering chain matrices and are given by the following:

$$S11D = -e^{2\gamma(l_l - l_{\text{open}})} \cdot q \cdot \frac{s}{p} \tag{4}$$

$$S21D = e^{\gamma(l_l + l_r - l_1)} \cdot \frac{r}{p} \tag{5}$$

$$S12D = e^{\gamma(l_l + l_r - l_1)} \cdot r \cdot \left[u + \frac{st}{p}\right] \tag{6}$$

$$S22D = -e^{-2\gamma(l_1 - l_r - l_{\text{open}})} \cdot \frac{r^2 \cdot t}{pq} \tag{7}$$

where

$$p = \frac{1}{y}\left(\frac{S11L}{x} - 1\right) \cdot T21M + \left(\frac{S11L}{x} - 1\right)\left(\frac{S22R}{y} - 1\right) \cdot T22M - \frac{T11M}{x \cdot y} - \frac{1}{x}\left(\frac{S22R}{y} - 1\right) \cdot T12M$$

$$q = \frac{1 + \frac{1}{x}(S110P - S11L)}{S110P - S11L}$$

$$r = \frac{T22M2 - T22M1 \cdot e^{-\gamma(l_2 - l_1)}}{2\sinh\gamma(l_2 - l_1)}$$

$$s = \frac{T11M}{y} + \left(\frac{S22R}{y} - 1\right) \cdot T12M - \frac{S11L}{y} \cdot T21M - S11L \cdot \left(\frac{S22R}{y} - 1\right) \cdot T22M$$

$$t = \frac{T11M}{x} + \frac{S22R}{x} \cdot T12M - \left(\frac{S11L}{x} - 1\right) \cdot T21M - S22R \cdot \left(\frac{S11L}{x} - 1\right) \cdot T22M$$

$$u = T11M + T12M \cdot S22R - T21M \cdot S11L - T22M \cdot S11L \cdot S22R$$

$$S11L = \frac{T12M1 \cdot e^{\gamma(l_1 - l_2)} - T12M2}{T22M1 \cdot e^{\gamma(l_1 - l_2)} - T22M2}$$

$$S22R = \frac{T11M1 \cdot e^{\gamma(l_1 - l_2)} - T11M2}{T12M2 - T12M1 e^{\gamma(l_1 - l_2)}}$$

$$x = \frac{T11M1 \cdot e^{\gamma(l_1 - l_2)} - T11M2}{T21M1 \cdot e^{\gamma(l_1 - l_2)} - T21M2} + \frac{T11M1 \cdot e^{-\gamma(l_1 - l_2)} - T11M2}{T21M2 - T21M1 \cdot e^{-\gamma(l_1 - l_2)}}$$

$$y = \frac{T11M1 \cdot e^{\gamma(l_1 - l_2)} - T11M2}{T12M2 - T12M1 \cdot e^{\gamma(l_1 - l_2)}} + \frac{T11M1 \cdot e^{-\gamma(l_1 - l_2)} - T11M2}{T12M1 \cdot e^{-\gamma(l_1 - l_2)} - T12M2}.$$

Here l_{open} is the length of the open line; l_l is the line length up to the reference plane on the left-hand side of the device; l_r is the line length up to the reference plane on the right-hand side of the device; and $TijM$ is the measured scattering chain matrix with the embedded device.

The expressions (4)–(7) are dependent on line length differences; so long as the discontinuity effects at the two launcher pin positions do not interact, we can consider the

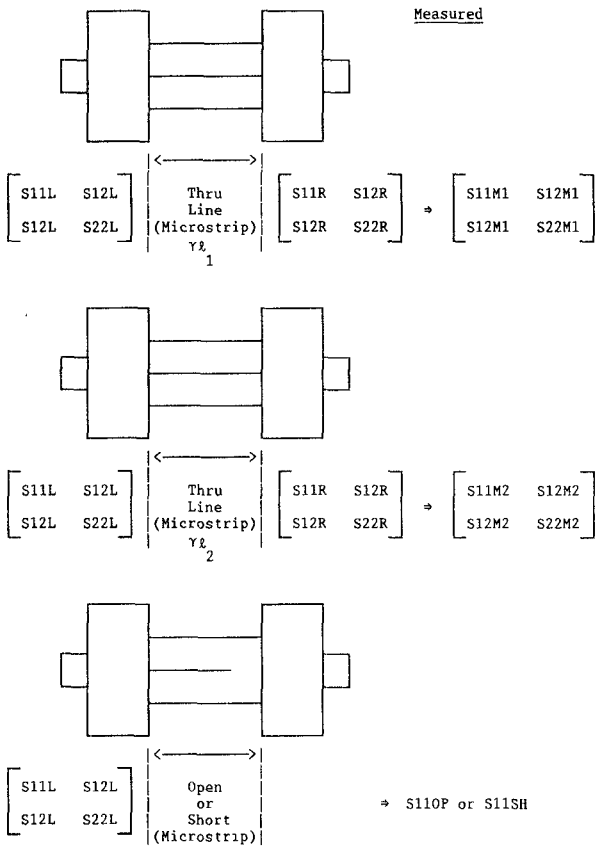

Fig. 1. Three sets of S parameter measurements with the end pieces of the fixture. It is assumed the transitions are reproduced quite accurately from one standard to the other. The transitional discontinuity is being absorbed in the S parameters of the end pieces.

physical lengths of the lines for our calculations. The line lengths l_r, l_l, and l_{open} can be arbitrary, as long as we avoid RF leakage [2].

The above-mentioned inequalities (2) and (3) can be used as checks (Appendix I) for choosing the correct angular rotation of expression (1). This will yield the correct sign for both α and β of the propagation constant. Sometimes measurement errors, combined with improper choices for the dimensions of through lines, will lead to some unrealistic values for α; α may become too large, sometimes negative, or it may vary randomly with frequency. If α is too large, it will show up in the de-embedded results, e.g., $(|S11|^2+|S12|^2)$ may become greater than 1 for a passive device. If α varies in a random fashion with frequency, the insertion loss of a de-embedded passive device,

$$\frac{|S21|^2}{1-|S11|^2}$$

will also vary in a random way with frequency. If α is negative, it is unrealistic. In Appendix II, we discuss how this error can be minimized by a proper choice of dimensions for the standard through lines.

III. Measurement

In keeping with the discussions in Appendix II, the through line dimensions are chosen to improve the certainties in $\text{Im}(A)$; $l_{\text{open}} = 0.1622$ in. The end effect length for the open-ended line is calculated from the expression in [9], with ϵ_{eff} values determined from (1). In Fig. 2, the fixture de-embedded S parameters of a MESFET device have been compared with those taken with RF probes directly on the wafer. The device was mounted on a carrier and then bonded to microstrip lines (25 mils wide) on 25 mil alumina substrate. The carrier was placed inside the end launchers. The data were de-embedded up to the bonding wire (included). So the de-embedded data will have the effect of bonding parasitics. By comparing these two sets of S parameters, the parasitics due to the bond wires, bonding pads, and via holes have been extracted. In Fig. 2(e), we show the complete model with the associated parasitics. This comparison is a good way of estimating the via hole inductances, which act as feedback elements and affect the response in a sensitive way. The value of via hole inductance listed in Fig. 2(e) is for a pair of via holes on 4 mil GaAs substrate. The parasitic model has been extracted by comparing the RF-probed and the de-embedded results at four bias points simultaneously. The comparison is shown for one bias point in Fig. 2(a)–(d).

Fig. 3 shows the sensitivity of the de-embedded results on the repeatability of the contacts between the launcher pins and the microstrip lines. Expressions (4)–(7) show that uncertainties in the determination of $S11L$ and $S22R$ will reflect the uncertainties in the de-embedded results, provided we can determine the propagation constant with good accuracy. An average value of $|S11L|$ and $|S22R|$ determined from four pairs of (l_1, l_2) has been perturbed by ± 30 percent in de-embedding a through line 0.3476 in long. The perturbation covers more than the observed values of $|S11L|$ and $|S22R|$. The maximum residual error in $|S21|$ is less than 0.2 dB and in $\angle S21$ less than 2.5° up to 20 GHz. Finally, we tabulate in Table I the de-embedded results of a multiturn (3.5 turn) spiral coil. We choose the pairs of lines as discussed in Appendix II. The de-embedded results are compared with those of another pair ($l_1 = 0.3979$ in, $l_2 = 0.4474$ in).

Table I shows that at all three frequencies the quantity $(|S11|^2+|S21|^2)$ has exceeded 1 when de-embedded with the pair ($l_1 = 0.3979$ in and $l_2 = 0.4475$ in). With the other set (as discussed in Appendix II), $(|S11|^2+|S21|^2)$ is less than 1. The value of α, as calculated from the pair (0.3979 in, 0.4475 in), was quite high at these frequencies (Fig. 4). This has led to incorrect de-embedded results. It can be concluded from Table I that it is important to calculate α properly. This error may not be serious in most of the measurements; it is, however, helpful to know about this discrepancy in the fixture de-embedding and apply the possible remedy.

The procedure described in the text for finding γ is nothing but a comparison method in which we try to identify and minimize the terms that introduce errors. The

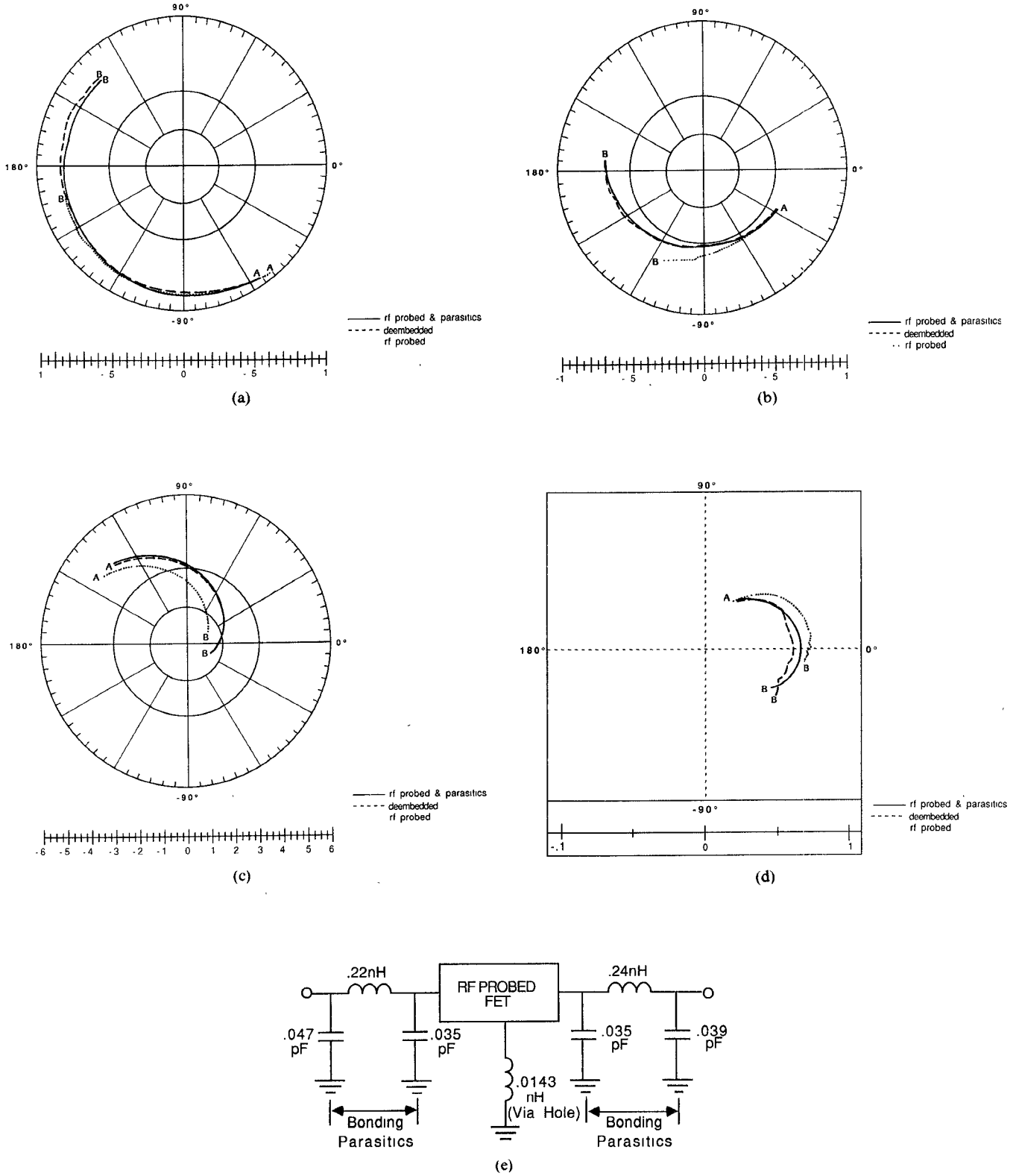

Fig. 2. Comparison of de-embedded FET data and RF-probed data on polar plot. The FET (F010-R310B) has a total gate periphery of 600 μm, biased at $V_D = 6$ V, $V_g = -1.0$ V, $I_{DS} = 111$ mA. The parasitics have been determined by fitting the two sets of S parameter data (RF-probed and de-embedded) simultaneously at four bias points. A: 2 GHz, B: 18 GHz. (a) $S11$. (b) $S22$. (c) $S21$. (d) $S12$. (e) RF-probed FET embedded in parasitics due to bond wires and via hole. This model has been fitted with the fixture–de-embedded S parameters.

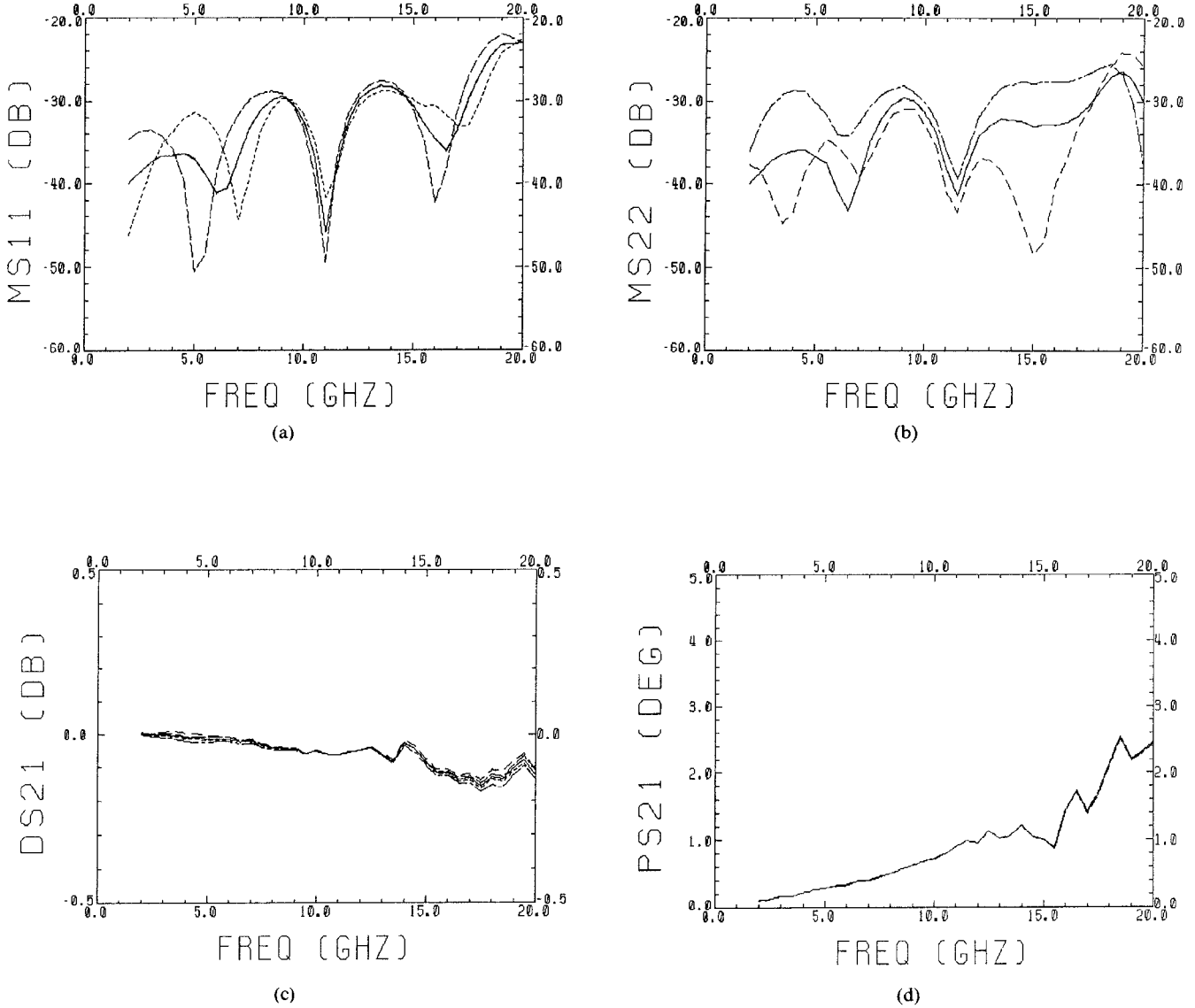

Fig. 3. Random residual errors for a through line (0.3476 in) on alumina substrate for ± 30 percent variation about the average values of $|S11L|$ and $|S22R|$. This variation covers more than the total spread of $|S11L|$ and $|S22R|$ calculated from the measurements with four pairs of (l_1, l_2). —— average $|S11L|$, $|S22R|$; ····· 1.3 $|S11L|$, $|S22R|$; – – – 0.7 $|S11L|$, $|S22R|$; –·–·– $|S11L|$, 1.3 $|S22R|$; ------- $|S11L|$, 0.7 $|S22R|$. (a) De-embedded $|S11|$. (b) De-embedded $|S22|$. (c) De-embedded $|S21|$. (d) De-embedded $\angle S21$.

TABLE I
MAGNITUDES OF S11 AND S21 OF A 3.5 TURN COIL (COIL 13-1)

Frequency (GHz)	Measured		De-embedded (l_1, l_2: Appendix II)		De-embedded ($l_1 = 0.3979$ in $l_2 = 0.4474$ in)	
	$\|S11\|$	$\|S21\|$	$\|S11\|$	$\|S21\|$	$\|S11\|$	$\|S21\|$
16	0.822	0.443	0.871	0.439	0.914	0.436
17	0.833	0.398	0.892	0.422	0.925	0.418
18	0.86	0.355	0.900	0.410	0.945	0.409

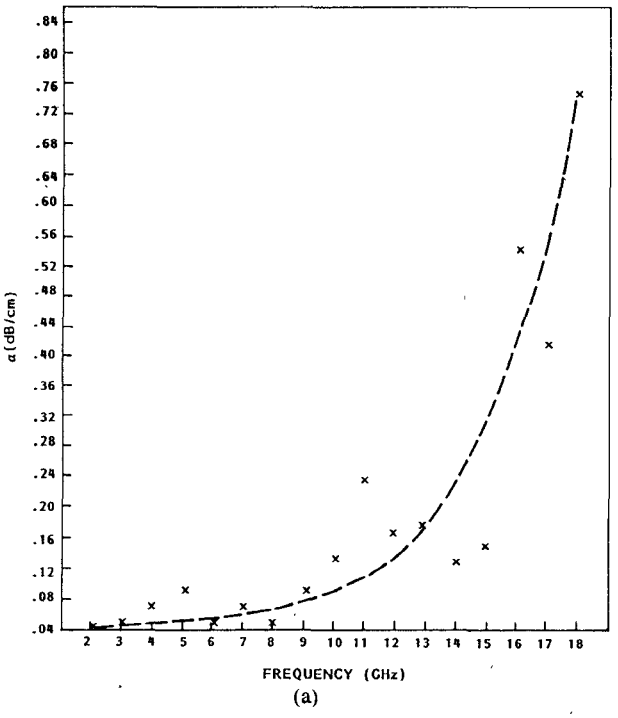

(a)

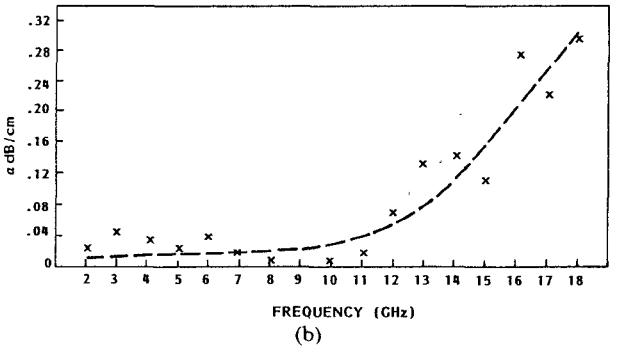

(b)

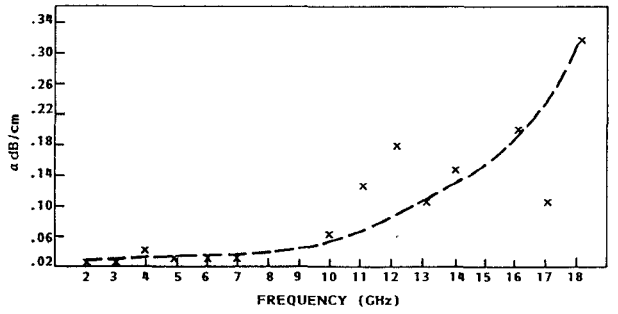

(c)

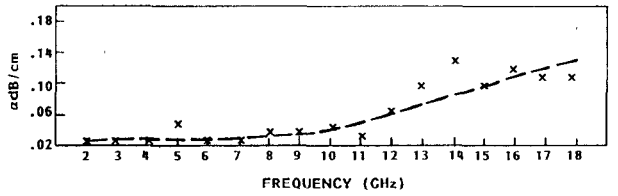

(d)

Fig. 4. Attenuation constant calculated from the measurement of different pairs of lines. (a) $l_1 = 0.4474$ in; $l_2 = 0.3979$ in. (b) $l_1 = 0.4474$ in; $l_2 = 0.3478$ in. (c) $l_1 = 0.2480$ in; $l_2 = 0.4474$ in. (d) $l_1 = 0.6177$ in; $l_2 = 0.240$ in.

comparison technique should produce a very fair estimate of $\alpha + j\beta$, because the systematic errors are canceled out [12].

IV. Conclusions

The through line dimensions should be properly chosen in the de-embedding of the microwave test fixtures. Otherwise, the quantity $\mathrm{Im}(A)$ can be erroneous. It will lead to two errors: (i) improper determination of α and (ii) wrong angular quadrant for $\arg(A)$. α may be high, as discussed above (Table I), or it may be negative (Appendix II). In our case, the second error will cause opposite signs for α and β. Since $\arg(A)$ is used to keep track of the proper rotation of the angle, $|\angle S21M1 - \angle S21M2|$, there will be error in the determination of β. If the error in α is tolerable, then it may be adequate to use just one pair of lines, which will avoid $|\angle S21M1 - \angle S21M2| \sim n\pi$ at the measurement frequencies. Although at $|\angle S21M1 - \angle S21M2| = (2n+1)\pi/2 \pm \epsilon$, $\mathrm{Re}(A)$ is in error, ϵ can be made negligible by maximizing the measurement certainty of $\mathrm{Im}(A)$. ϵ is also minimized by using a fixture with low reflection coefficients.

Appendix I

Under the following assumptions:

$$|S11M1| \simeq 0,\ |S22M1| \simeq 0,$$

$$|S11M2| \simeq 0, \text{ and } |S22M2| \simeq 0$$

the expression for A can be rewritten as follows:

$$\mathrm{Re}(A) \simeq \left(\frac{|S12M1|}{|S12M2|} + \frac{|S12M2|}{|S12M1|}\right) \cdot \cos(\angle S12M1 - \angle S12M2) \tag{A1}$$

$$\mathrm{Im}(A) \simeq \left(\frac{|S12M1|}{|S12M2|} - \frac{|S12M2|}{|S12M1|}\right) \cdot \sin(\angle S12M1 - \angle S12M2). \tag{A2}$$

If α is small (in most cases it is a valid assumption), then $|S12M1|$ is close to $|S12M2|$; it is then relatively easy to show the following (except at $|\angle S12M1 - \angle S12M2| = (2n+1)\pi/2$):

$$\frac{A \pm \sqrt{A^2 - 4}}{2} \simeq \frac{1}{2}\left(\frac{|S12M1|}{|S12M2|} + \frac{|S12M2|}{|S12M1|}\right) \cdot \left[\cos(\angle S12M1 - \angle S12M2) \pm j\sqrt{\sin^2(\angle S12M1 - \angle S12M2)}\right]. \tag{A3}$$

The magnitude of (A3) is greater than 1. When

$$0 < (l_1 - l_2) < \frac{\lambda e}{4}$$

the expression (A3) can be rewritten with the positive sign as

$$\frac{A + \sqrt{A^2 - 4}}{2} \simeq \frac{1}{2}\left(\frac{|S12M1|}{|S12M2|} + \frac{|S12M2|}{|S12M2|}\right) \cdot e^{j(\angle S12M2 - \angle S12M1)}. \quad \text{(A4)}$$

If

$$\frac{\lambda e}{4} < (l_1 - l_2) < \frac{\lambda e}{2}$$

the negative sign in front of the square root will put the angle in the right quadrant, which is

$$\frac{\pi}{2} < (\angle S12M2 - \angle S12M1) < \pi.$$

So, (A3) can be written as

$$\frac{A - \sqrt{A^2 - 4}}{2} \simeq \frac{1}{2}\left(\frac{|S12M1|}{|S12M2|} + \frac{S12M2|}{|S12M1|}\right) \cdot e^{j(\angle S12M2 - \angle S12M1)}$$

$$\text{when } \frac{\lambda e}{4} < (l_1 - l_2) < \frac{\lambda e}{2}. \quad \text{(A5)}$$

If we examine (A1) and (A2), $\mathrm{Re}(A)$ and $\mathrm{Im}(A)$ are both positive when

$$0 < (l_1 - l_2) < \frac{\lambda e}{4}$$

and $\mathrm{Re}(A)$ is negative and $\mathrm{Im}(A)$ is positive when

$$\frac{\lambda e}{4} < (l_1 - l_2) < \frac{\lambda e}{2}.$$

So, the arguments of A can be used as a flag for choosing the right sign. In the present de-embedding procedure, $\arg(A)$ is used to keep track of the correct angular rotation of expression (1) given in the text. This is a fairly good check provided the assumptions mentioned in this appendix are satisfied. This is further discussed in Appendix II.

Appendix II

The expression for $\mathrm{Im}(A)$ can be written as follows:

$$\begin{aligned}\mathrm{Im}(A) = &\left(\frac{|S12M1|}{|S12M2|} - \frac{|S12M2|}{|S12M1|}\right) \cdot \sin(\angle S12M1 - \angle S12M2) \\ &- \frac{|S11M1| \cdot |S22M1|}{|S12M1| \cdot |S12M2|} \cdot \sin[(\angle S11M1 + \angle S22M1) - (\angle S12M1 + \angle S12M2)] \\ &- \frac{|S11M2| \cdot |S22M2|}{|S12M1| \cdot |S12M2|} \cdot \sin[(\angle S11M2 + \angle S22M2) - (\angle S12M1 + \angle S12M2)] \\ &- \frac{|S22M1| \cdot |S11M2|}{|S12M1| \cdot |S12M2|} \cdot \sin[(\angle S22M1 + \angle S11M2) - (\angle S12M1 + \angle S12M2)] \\ &- \frac{|S11M1| \cdot |S22M2|}{|S12M1| \cdot |S12M2|} \cdot \sin[(\angle S11M1 + \angle S22M2) - (\angle S12M1 + \angle S12M2)]. \end{aligned} \quad \text{(A6)}$$

If l_1 and l_2 are chosen close to each other but $l_1 > l_2$, then the sign of $\mathrm{Im}(A)$ may become erroneous under the following cases:

i) Due to a small value of α, $|S12M1|$ may be erroneously measured greater than $|S12M2|$; it will change the sign of the first term.
ii) $|\angle S12M1 - \angle S12M2|$ is close to 0 or π; so the first term is very small.
iii) High value of reflection (a good upper limit being the product of any two reflection magnitudes smaller than $|S12M1|^2 - |S12M2|^2$), with associated error in the measurement of their angles; this upper limit is not very high, and it is easy to make errors in the measurement of the angles.

Considering the above three reasons, it is advisable to maximize the first term of $\mathrm{Im}(A)$, because all terms in the first term can be measured with the best possible certain-

TABLE II

Frequency (GHz)	1–5	6–7	8–11	12–13	14–17	18
l_1	0.6177	0.4474	0.6177	0.4474	0.6177	0.4474
l_2	0.248	0.248	0.248	0.3478	0.248	0.248

l_1 and l_2 are in in. The substrate is 25 mil alumina with 25 mil wide microstrip line.

ties. Our objective will be to choose the through line dimensions in such a way as to avoid $\Delta\theta = |\angle S12M1 - \angle S12M2| \sim n\pi$ at the measurement frequencies. In the present de-embedding procedure, the phase difference is approximately maintained within the range

$$\left(n\pi + \frac{\pi}{6}\right) \leqslant \Delta\theta \leqslant \left((n+1)\pi - \frac{\pi}{6}\right).$$

The lengths l_1 and l_2 are chosen conveniently to improve the measurement certainties of

$$\left(\frac{|S12M1|}{|S12M2|} - \frac{|S12M2|}{|S12M1|}\right).$$

The value of $|l_1 - l_2|$ should not be too small, then $|S12M1| \simeq |S12M2|$; on the other hand, $|l_1 - l_2|$ should not be too large, then the difference $|l_1 - l_2|$ is to be changed quite frequently when $\Delta\theta$ is not within the above mentioned range. In Fig. 4, the calculated values of α from expression (1) in the text have been plotted for various (l_1, l_2) pairs. These values may be compared with the theoretical data [10] and the experimental data [11]. Even though the values of α calculated herein with frequency show a convexity opposite to that predicted [10], Fig. 4(d) has been chosen to represent α because they come close to the predicted values [10]. At the frequencies where $\Delta\theta$ is not within our range, l_1 and l_2 are chosen differently. Table II shows the line lengths chosen over the frequency range 2 to 18 GHz with 1 GHz steps. When Fig. 4(a) was chosen to represent α, the de-embedded results of a few passive devices (coils in our case) did not satisfy the condition $(|S11|^2 + |S12|^2) < 1$ at higher frequencies. In Fig. 4, a few data points are missing, for example, at 8 and 9 GHz in Fig. 4(b) and at 9 GHz in Fig. 4(c). The calculated values of α are negative at these frequencies. This is because of the error in $\mathrm{Im}(A)$. The dashed lines in the figure show an average trend of α with frequency. The actual values used in the de-embedding procedure are those shown by X.

Lastly, it should be noted that we have mainly discussed the imaginary part of A. As for $\mathrm{Re}(A)$, the main term, as shown in (A1), tends to zero as $\Delta\theta \to (2n+1)\pi/2$. When the imaginary part of A is maximized, the coefficient of $\cos\Delta\theta$ in (A1) is also maximized. The other terms in $\mathrm{Re}A$ have the same coefficients as those from the second to the fourth terms in (A6). These coefficients are negligible compared to the first term coefficient of $\mathrm{Re}(A)$ in (A1). Unless $\Delta\theta$ is very close to $(2n+1)\pi/2$, $\mathrm{Re}(A)$ will have the correct sign, and $\arg(A)$ can be used as a flag for checking the angular rotation of A.

ACKNOWLEDGMENT

The authors are thankful to L. Rider and A. Jabra for helpful suggestions. They also wish to thank Dr. Duh for initiating the work.

REFERENCES

[1] N. R. Franzer and R. A. Speciale, "New procedure for system calibration and error removal in automated *S*-parameter measurements," in *Proc. 5th European Microwave Conf.*, 1975, pp. 69–73.
[2] R. A. Speciale, "A generalization of the TSD network analyzer calibration procedure, covering *n*-port scattering parameter measurements, affected by leakage errors," *IEEE Trans. Microwave Theory Tech.*, vol. MTT-25, pp. 1100–1115, Dec. 1977.
[3] B. Bianco *et al.*, "Launcher and microstrip characterization," *IEEE Trans. Instrum. Meas.*, vol. IM-25, no. 4, pp. 320–323, Dec. 1976.
[4] M. Hillbun, "Enhance *S*-parameter accuracy," *Microwave System News*, pp. 83–93, Mar. 1980.
[5] D. Swanson, "Ferret out fixture errors with careful calibration," *Microwaves*, pp. 79–85, Jan. 1980.
[6] S. E. Rosenbaum *et al.*, "A calibration method for deembedding a microwave test fixture," in *27th Automatic RF Tech. Conf. Dig.*, 1986, pp. 148–158.
[7] J. Standinger, "MMIC tests improved with standards on chip," *Microwaves and RF*, pp. 107–114, Feb. 1987.
[8] J. Curran, "Network analysis of fixtured devices," in *Hewlett Packard RF & Microwave Measurement Symp.*, Sept. 1986, paper #6.
[9] M. Kirschring *et al.*, "Accurate model for open end effect of microstrip lines," *Electron. Lett.*, vol. 17, no. 3, pp. 123–125, Feb. 5, 1981.
[10] R. H. Jansen, "High speed computation of single and coupled microstrip parameters including dispersion, high order modes, loss and finite strip thickness," *IEEE Trans. Microwave Theory Tech.*, vol. MTT-26, pp. 75–82, Feb. 1978.
[11] R. A. Pucel *et al.*, "Losses in microstrip," *IEEE Trans. Microwave Theory Tech.*, vol. MTT-16, pp. 342–350, June 1968.
[12] K. Gupta *et al.*, *Microstriplines and Slotlines*. Dedham, MA: Artech House, 1979, ch. 1, p. 35.

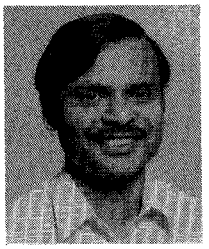

Jyoti P. Mondal (S'82–M'84) was born in Calcutta, India. He received the bachelor of technology degree in electronics and electrical communication engineering from the Indian Institute of Technology, Kharagpur, in 1977 and the M.S. and Ph.D. degrees, both in electrical engineering, from Carnegie-Mellon University, Pittsburgh, in 1981 and 1984, respectively.

From 1977 to 1980, he worked with Bharat Electronics Limited, Ghaziabad, India, as an R&D Engineer, developing bipolar power and

low-noise amplifier circuits in the *L*-band. His project and thesis work for the M.S. and Ph.D. degrees included variable-gain amplifiers and monolithic phase shifters for *S*-band applications. Since 1984, he has been employed by the General Electric Company, Electronics Laboratory, Syracuse, NY. His present activities are mainly in the microwave monolithic circuit area, involving RF circuits, device physics, and measurement techniques.

✠

Tzu-Hung Chen (S'83–M'84) was born in Taiwan, Republic of China, on May 17, 1954. He received the B.Ed. degree in physics from National Taiwan College of Education in 1976, the M.S. degree in physics from National Taiwan Normal University in 1978, and the Ph.D. in electrical engineering from the University of Minnesota in 1984. His graduate study at the University of Minnesota was on GaAs device modeling and circuit simulation.

He spent two years at the Electronics Laboratory of General Electric involved in MMIC design and device characterization and modeling. Since 1987, he has been with Microwave Semiconductor Corp., Somerset, NJ, where he continues his efforts on MMIC design and device design and characterization.